Available online at www.sciencedirect.com
ScienceDirect
Materials Chemistry and Physics 109 (2008) 174–180
MATERIALS CHEMISTRY AND PHYSICS
www.elsevier.com/locate/matchemphys

Review

XRD, XPS and SEM characterisation of Cu–NbC nanocomposite produced by mechanical alloying

M.T. Marques [a,*], A.M. Ferraria [b], J.B. Correia [a], A.M. Botelho do Rego [b], R. Vilar [c]

[a] *INETI-DMTP, Estrada do Paço do Lumiar 22, 1649-038 Lisboa, Portugal*
[b] *IST, Centro de Química-Física Molecular, Av. Rovisco Pais, 1049-001 Lisboa, Portugal*
[c] *IST, Dep. Eng. de Materiais, Av. Rovisco Pais, 1049-001 Lisboa, Portugal*

Received 2 April 2007; received in revised form 10 October 2007; accepted 21 October 2007

Abstract

In situ formation of NbC in nanocomposite copper powders was achieved by mechanical alloying at room temperature without further heat treatment. Nominal compositions of 10 and 20 vol.% of NbC were produced from elemental powders of copper, graphite and niobium for milling times of 3.6, 7.2, 14.4, 28.8, 57.6 and 115.2 ks. As-milled Cu–NbC nanocomposites were characterised by scanning electron microscopy (SEM), X-ray diffraction (XRD) and X-ray photoelectron spectroscopy (XPS). XRD and XPS results show that NbC begins to form during the first 3.6 ks, and increases with the time of milling. The kinetics of NbC formation was studied using the results obtained from XRD and XPS experiments. A mechanism for the synthesis of NbC is proposed.
© 2007 Elsevier B.V. All rights reserved.

Keywords: Composite materials; Powder metallurgy; XRD; XPS

Contents

1. Introduction

High strength and high electrical and thermal conductivity Cu-based alloys are prime candidates for applications such as spot welding electrodes, high-performance switches, rotating source neutron targets, combustion chamber liners and nozzle liners [1,2]. Mechanical alloying (MA) is one of the most promising techniques used to produce heat-resistant dispersion-strengthened copper alloys. MA [3] can also be successfully used to produce *in situ* Cu-matrix composites reinforced with particles of materials such as borides, carbides, oxides and intermetallic compounds [1,2,4–11]. The repeated deformation, welding and fracturing that occur in MA lead to an intimate mixing of the components. Additional heat treatment is usually required to promote the precipitation of fine particles of reinforcement phases such as carbides, oxides and nitrides in the metal matrix. Recently Marques et al. have synthesised Cu–NbC nanocomposites by MA, without further heat treatment being required to achieve a suitable microstructure and properties [12]. The early stages of the process were investigated in order to reveal the mechanisms of *in situ* formation of NbC within the copper matrix [13]. Compared to other methods, *in situ* synthesis by MA offers advantages such as more uniform reinforcement particle distribution and finer particle size, leading to stronger

* Corresponding author. Tel.: +351 217 165 141; fax: +351 217 166 568.
E-mail addresses: tmarques@ineti.pt (M.T. Marques), ana.ferraria@ist.utl.pt (A.M. Ferraria), brito.correia@ineti.pt (J.B. Correia), amrego@ist.utl.pt (A.M.B.d. Rego), rui.vilar@ist.utl.pt (R. Vilar).

0254-0584/$ – see front matter © 2007 Elsevier B.V. All rights reserved.
doi:10.1016/j.matchemphys.2007.10.032

and more heat-resistant materials. In the present work, mixtures of Cu, C and Nb powders corresponding to nominal contents of 10 and 20 vol.% of NbC produced by MA were characterised by X-ray diffraction (XRD), scanning electron microscopy (SEM) and X-ray photoelectron spectroscopy (XPS) in order to reveal the mechanisms and kinetics of *in situ* formation of NbC during mechanical alloying.

2. Experimental

Copper-based nanocomposite powders reinforced with NbC were synthesised *in situ* by mechanical alloying. Mixtures corresponding to nominal contents of 10 and 20 vol.% NbC were produced from powders of Cu (99.9% purity; particle size 44 μm < *d* < 149 μm), Nb (99% purity; average particle size 65 μm) and synthetic graphite (99.9995% purity; average particle size 74 μm). The milling was performed in two steps. Firstly, a mixture of Cu and graphite powders was milled for 14.4 ks to produce a Cu–C pre-alloyed powder. This step has two main objectives, to deoxidise the Cu and to disperse graphite into the copper matrix. In the second step (NbC synthesis), Nb was added to the mixture and milling continued for different times, namely 0.9, 3.6, 7.2, 14.4, 28.8, 57.6 and 115.2 ks. A detailed account of the material preparation method has been reported elsewhere [12].

The materials were characterised by X-ray diffraction (XRD), scanning electron microscopy (SEM) and X-ray photoelectron spectroscopy (XPS). XRD was performed with a Rigaku Geigerflex diffractometer fitted with a graphite monochromator in the diffracted beam, using Cu Kα radiation. Scanning speeds of 0.02 and 0.006° min^{-1} (2θ) were used for fast acquisition of complete spectra and high resolution scanning of (1 1 1) Cu and (1 1 1) NbC peaks (in the 32–54° 2θ range), respectively. The volume fraction of NbC was calculated from the ratio of (1 1 1) NbC and (1 1 1) Cu peaks, I_{NbC}/I_{Cu}. Samples for SEM observation were prepared by mounting the powders in conductive resin and polishing using a standard technique. The observations were carried out in a Philips XL30 FEG with EDS analysis. The X-ray photoelectron spectrometer used was an XSAM800 (KRATOS) model operated in fixed analyser transmission (FAT) mode with pass energy of 20 eV. Non-monochromatic Mg Kα and Al Kα X-radiation (hν = 1253.6 and 1486.6 eV, respectively) were used. The power was set to 130 W. Powder samples were compacted to pellets and mounted with double-sided adhesive carbon tape. The samples were introduced into spectrometer under a pure nitrogen flux and analysed in an ultrahigh-vacuum (UHV) chamber (~10^{-7} Pa) at room temperature with a take-off angle (TOA) of 45°. The spectra were recorded on a Sun SPARC Station 4 with Vision software (KRATOS), using increments of 0.1 eV. X-ray source satellites were subtracted. A Shirley background was used for the baseline subtraction. Peak fitting was carried out with a non-linear least-squares algorithm using pseudo-Voigt profiles (Gaussian/Lorentzian (GL) products). No flood gun was used for charge compensation. For samples containing copper + graphite(+niobium), the charge shift was corrected using the binding energy of graphite C 1s (284.4 eV). This value resulted from the charge correction performed on the spectrum of graphite, considering that the oxygen present in pure graphite is from physisorbed moisture and is centred at 532.0 eV [14]. For niobium, copper oxide (Cu_2O) and pristine copper powders the charge shift was corrected using as reference the binding energy of aliphatic C 1s (285 eV), while for NbC powder the charge shift was corrected using the energy of Nb $3d_{5/2}$ in NbC (203.7 eV) [15–17]. The sensitivity factors used for quantification purposes were 6.3 for Cu $2p_{3/2}$, 2.4 for Nb 3d, 0.66 for O 1s and 0.25 for C 1s.

3. Results

The milled samples were first observed by SEM. The microstructure of Cu–20NbC powder milled for 0.9 ks observed in backscattered electron mode (BSE) and the EDS spectra obtained in the regions identified as a1 and a2 are depicted in Fig. 1. The corresponding microstructure is typical of very early stages of milling, and shows the beginning of Nb and Cu mixing. Chemical analysis performed on large bright particles (a1) shows that these correspond to pure Nb (a1), while the dark

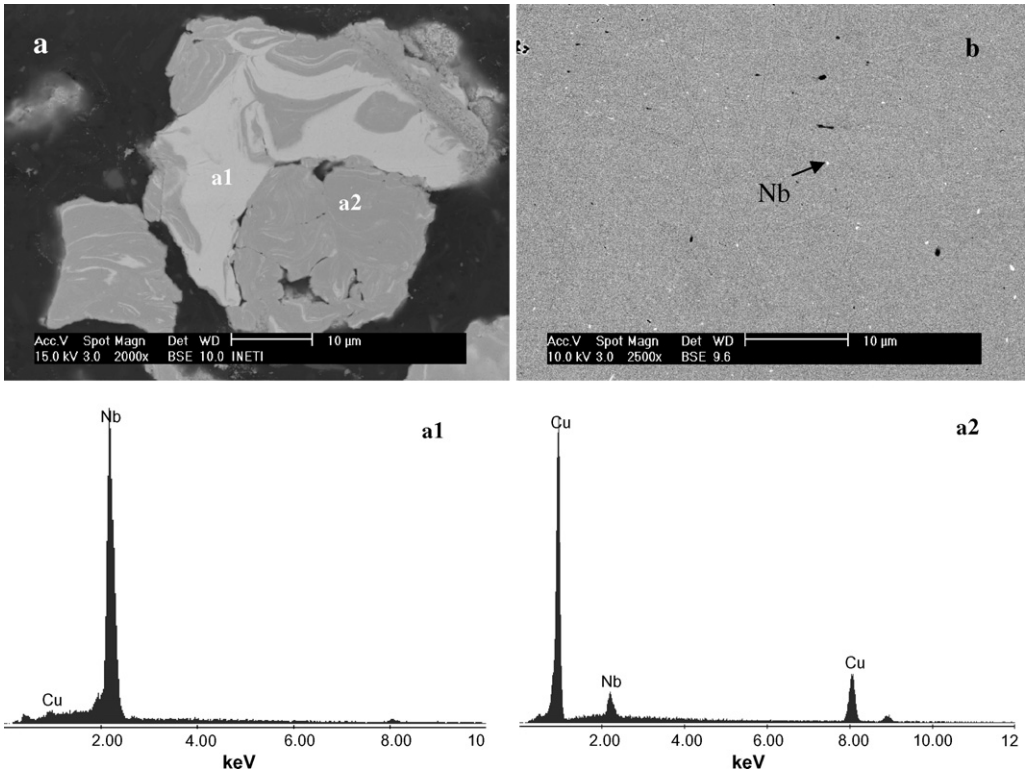

Fig. 1. SEM images of Cu–20NbC powders milled for (a) 0.9 ks and (b) 3.6 ks. Spectra labelled a1 and a2 correspond to chemical analysis performed in regions labelled a1 and a2, respectively.

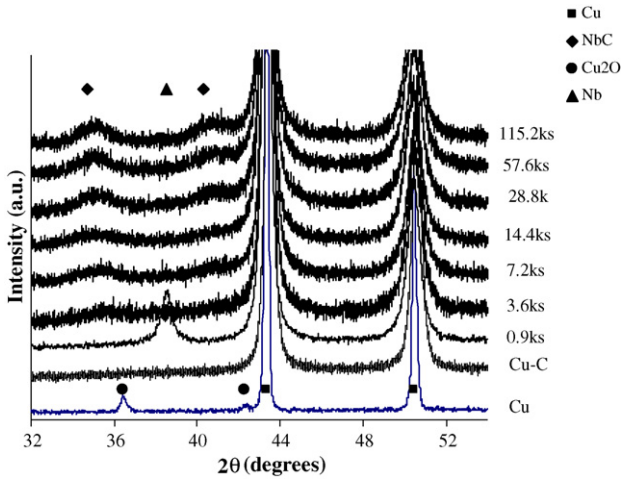

Fig. 2. X-ray diffractograms of the as-milled Cu powders with 10 vol.% of NbC. Cu corresponds to Cu starting powder and Cu–C corresponds to pre-alloyed powders.

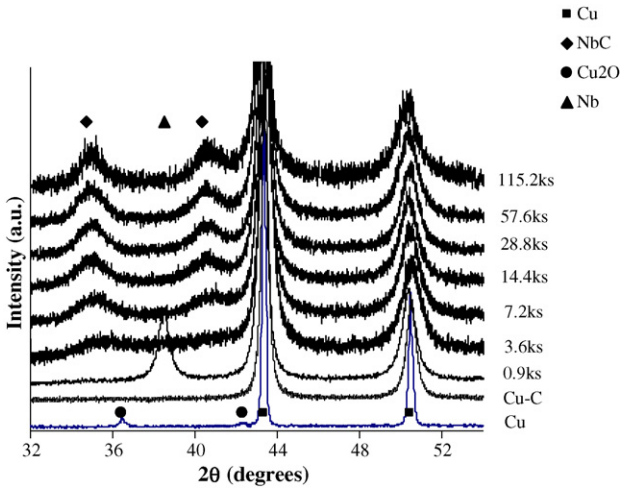

Fig. 3. X-ray diffractograms of the as-milled Cu powders with 20 vol.% of NbC. Cu corresponds to Cu starting powder and Cu–C corresponds to pre-alloyed powders.

ones (a2) correspond to a mixture of Cu, C and Nb resulting from milling (a2). A lamellar structure typical of mechanical alloying and of ductile metals subjected to repeated welding and fracturing during the process is also observed. The micrograph in Fig. 1(b) shows the microstructure of the powder milled for 3.6 ks. It consists of Nb (bright) about 400 nm in size dispersed in a homogeneous matrix. The microstructure becomes entirely homogeneous for milling times longer than 28.8 ks.

The diffractograms of milled Cu–10NbC and Cu–20NbC powders in the range of 32–54° (2θ) are shown in Figs. 2 and 3, respectively. The diffractogram of a Cu powder is also included for comparison. As expected, the intensity of NbC peaks increases with increasing milling time and increasing proportion of NbC. This compound can only be detected for milling times exceeding a few hours (>7.2 ks), independently of the sample composition.

The kinetics of NbC formation was studied by XPS for Cu–10NbC. Fig. 4 shows spectra of Cu powders in the pristine condition, of a Cu–C powder mixture milled for 14.4 ks and Cu_2O, (for reference purposes).

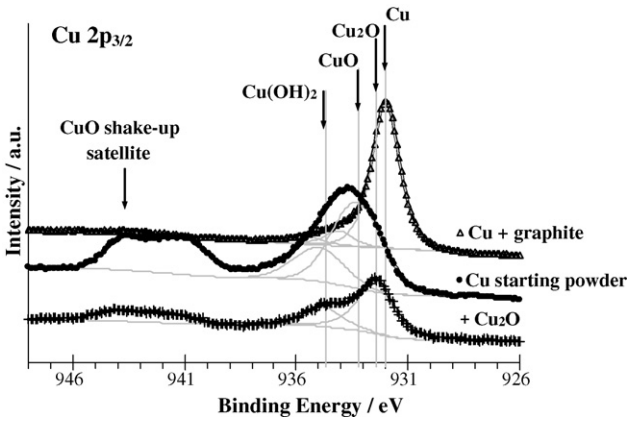

Fig. 4. Cu $2p_{3/2}$ XPS regions of reference powders: Cu_2O, Cu (starting powder) and Cu milled with graphite.

The XPS spectra show that pristine copper powders are oxidised (Fig. 4). The Cu $2p_{3/2}$ peak of the corresponding spectrum, centred at 933.3 eV, is wider than the main component of the other spectra (full width at half maximum (FWHM) is 2.7, 1.9 and 1.4 eV for Cu, Cu_2O and Cu–C powders, respectively). In fact, this peak includes several unresolved components, namely Cu^{2+} (CuO) at 933.2 eV [15,18], Cu^+ (Cu_2O) at 932.4 eV (main component in Cu_2O spectrum) and Cu^0 (metallic Cu), which presents a very similar binding energy to Cu_2O [15]. The second fitted component in the copper powder spectrum, centred around 935 eV, is assigned to copper bound to hydroxyl groups. The same form of copper is also present in the Cu_2O spectrum (peak centred at 934.7 eV). At higher binding energies, between 939 and 945 eV, high energy satellite structures are found, which are associated with Cu^{2+} species. The main component in the Cu + graphite spectrum, centred at 932.0 eV, can be assigned to Cu^+ (Cu_2O) and/or to Cu^0 (metallic Cu) [15], but the calculated Auger Parameter (AP), AP-$2p_{3/2}$, $L_3M_{45}M_{45}$ = 1851.0 eV indicates that this peak corresponds to metallic Cu (Cu^0). In the Cu_2O powder AP-$2p_{3/2}$, $L_3M_{45}M_{45}$ = 1849.5 eV is assigned to Cu_2O (Cu^+) [15].

Fig. 5 presents the Nb 3d region of Nb and NbC powders. The Nb 3d peak is a doublet with a 2.6 eV split. In what follows, only the binding energies of $3d_{5/2}$ will be mentioned. The spectra show that the outermost layers of these powders are composed mainly of Nb_2O_5, which corresponds to a peak centred at 207.1 eV. The Nb powder spectrum also shows the peak of metallic niobium (Nb^0) at 202.4 eV and a peak at 204.5 eV that may correspond to NbO or niobium oxicarbides ($NbC_{1-x}O_x$). In the NbC powder spectrum the peak at 203.7 eV is assigned to Nb–C.

The relative intensities of Cu^{2+} components decrease with milling time, while those assigned to Cu^+ and/or Cu^0 increase (Fig. 6). Simultaneously, the relative intensity of the components corresponding to NbC, at 203.8 ± 0.2 eV, increases with time (Fig. 7). As in Nb and NbC reference powders, Nb_2O_5 is also present, with a component at 207.0 ± 0.2 eV, but in milled powders the dominant oxide is at 206.2 ± 0.2 eV (labelled (2)

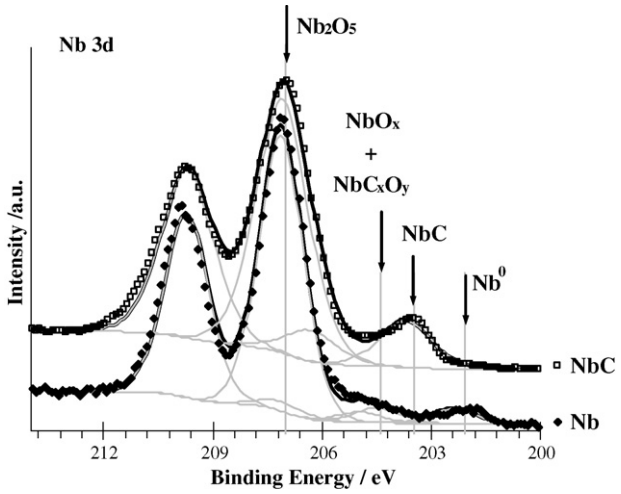

Fig. 5. Nb 3d XPS regions of reference powders: Nb and NbC. The arrows indicate Nb $3d_{5/2}$ components. Doublet separation ($3d_{3/2}$–$3d_{5/2}$) was fixed at 2.6 eV. Doublet intensity ratio I(Nb $3d_{5/2}$)/I(Nb $3d_{3/2}$) = 1.5. FWHM and GL (Gaussian/Lorentzian products) are the same for all the components of a XPS region.

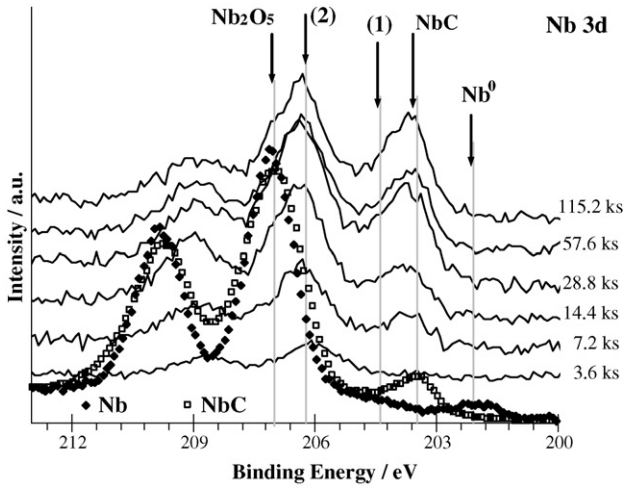

Fig. 7. XPS Nb 3d region for milling times of 3.6, 7.2, 14.4, 28.8, 57.6 and 115.2 ks. For comparison purposes the spectra of reference powders are presented: (♦) Nb and (□) NbC. For (1) and (2) assignments see text. The arrows indicate Nb $3d_{5/2}$ components.

in Fig. 7) which is assigned to NbO_2 or NbO_x with $2 < x < 2.5$ [15,19]. All Nb 3d regions were fitted with three doublets, corresponding to NbC, NbO_2 and Nb_2O_5, but the possibility of there being a fourth doublet must be considered. This doublet has its $3d_{5/2}$ component centred at 204.7 eV (indicated by (1) in Fig. 7) and is assigned to NbO or NbO_x with $1 < x < 2$ and/or to the oxicarbides $NbC_{1-x}O_x$ [15,16,20] as seen above for NbC reference powders.

The XPS results were obtained by analysing the evolution of Nb 3d peaks. The NbC fraction is given by the ratio between the area of the first doublet assigned to niobium bound to carbon (binding energy (Nb $3d_{5/2}$) = 203.8 ± 0.2 eV) and Nb_{total}, the total XPS niobium area. The quantitative of X-ray diffraction analysis was performed using the direct comparison method [21]. The fraction of NbC, f_{NbC}, was estimated by solving the system (1):

$$\frac{f_{NbC}}{f_{Cu}} = \frac{R_{Cu}}{R_{NbC}} \times \frac{I_{NbC}}{I_{Cu}}, \qquad f_{NbC} + f_{Cu} = 1 \tag{1}$$

with

$$R = \frac{1}{v^2}\left[|F|^2 p \left(\frac{1+\cos^2 2\theta}{\sin^2\theta\cos\theta}\right)\right] \exp(-2M) \tag{2}$$

where v is the unit cell volume, p the multiplicity factor, F the structure factor, $(1+\cos^2 2\theta)/(\sin^2\theta\cos\theta)$ the Lorentz-polarization factor, θ the Bragg angle and $\exp(-2M)$ the temperature factor. The values of R for NbC and Cu were determined taking F(Cu) = 86.4, F(NbC) = 114.8, p = 8. The temperature factor for copper ($\exp(-2M)$ (Cu) = 0.94) and niobium carbide ($\exp(-2M)$ (NbC) = 0.99) was calculated at T = 298 K using the Bragg angle corresponding to the (1 1 1) diffraction peak of Cu and NbC and the tabulated values of the characteristic Debye temperature for copper [21] and $NbC_{0.96}$ [22,23]. The unit cell volume of Cu was calculated using the Cu lattice parameter determined for each powder sample, as previously reported [13]. In the case of NbC the unit cell volume was determined assuming the tabulated value for the lattice parameter of NbC, 0.44690 nm [24]. Fig. 8 presents the volume fraction of NbC as a function of the milling time. The kinetics of NbC formation in the copper matrix was derived from XRD and XPS data. This kinetics is well described by an exponential equation such as

$$x = a(1 - \exp(-kt)) \tag{3}$$

where x is the volume fraction transformed at time t, k is the energy-dependent rate constant and a is a fitting parameter. Table 1 shows the values of k and a obtained by fitting of the experimental data to Eq. (3).

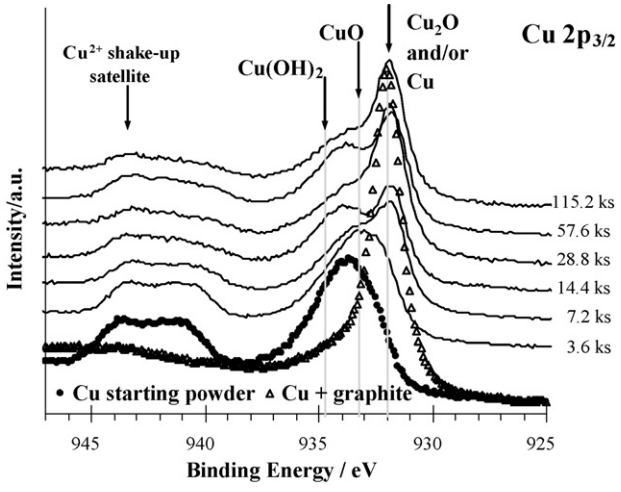

Fig. 6. XPS Cu $2p_{3/2}$ region for milling times of 3.6, 7.2, 14.4, 28.8, 57.6 and 115.2 ks. For comparison purposes the spectra of reference powders are presented: • Cu starting powder and ▲ Cu + graphite.

Table 1
Kinetics parameters obtained for the as-milled Cu powders with 10 and 20 vol.% of NbC from XRD and XPS techniques

Sample	Technique	k (ks^{-1})	a
Cu 10 vol.% NbC	XPS	$9.6 \times 10^{-2} \pm 0.02$	0.51 ± 0.04
	XRD	$1.6 \times 10^{-1} \pm 0.02$	0.74 ± 0.03
Cu 20 vol.% NbC	XRD	$1.9 \times 10^{-1} \pm 0.01$	0.88 ± 0.01

4. Discussion

During the milling process powder particles are subjected to high-energy collisions, which cause intense plastic deformation, manifested by a high density of defects such as dislocations and stacking faults, followed by fracture and cold welding between particles. Plastic deformation and cold welding predominate during the early stages of milling. Deformation leading to changes in particle shape and cold welding to an increase in particle size and the formation of a layered structure consisting of various combinations of the starting powders [25]. Fig. 1 shows two important steps in the mechanical synthesis of niobium carbide in the copper matrix. The powder particles shown in Fig. 1(a) present a typical layered structure formed as a result of ball milling. At this early stage of milling, just 0.9 ks after the addition of Nb, the matrix (dark regions labelled a2 in Fig. 1) is already relatively even but overall the structure is inhomogeneous. Chemical analysis performed in this area reveals a strong Nb peak, indicating some degree of mixing of the three components. This is more evident in Fig. 1(b), corresponding to Cu powders with 20 vol.% of NbC milled for 3.6 ks, in which fewer and smaller Nb particles are dispersed in a homogeneous matrix. No Nb-rich particles are observed by SEM for milling times longer than 28.8 ks. Figs. 2 and 3 show the X-ray diffractograms of samples with 10 and 20 vol.% of NbC milled for different times. The diffractograms of the Cu powder used as starting material were included for comparison. The presence of the two strongest Cu_2O diffraction peaks shows that the Cu powder used is oxidised; no other types of Cu oxide were detected. The X-ray diffractogram labelled Cu–C refers to a Cu + graphite powder mixture milled for 14.4 ks. The pre-alloying step is essential because the presence of oxygen in the mixture prevents NbC formation. If the Cu powder is excessively oxidised the product formed is Nb_XO_Y or Nb_XCO_Y instead of NbC. This occurs because niobium oxidises more easily than copper ($\Delta G_f(Nb_2O_5) = -1765\ kJ\ mol^{-1}$ and $\Delta G_f(Cu_2O) = -148\ kJ\ mol^{-1}$ at 300 K [26]). The X-ray diffractogram shows that Cu_2O diffraction peaks are absent from the pre-alloyed powder mixture (Figs. 2 and 3). The reducing effect of carbon was confirmed by XPS. The XPS features in Fig. 4, between 939 and 945 eV, are characteristic of Cu^{2+} compounds and arise from a multiplet splitting effect due to the interaction between the 2p core hole and the $3d^9$ electronic configuration in the final state of the photoemission process [20]. The spectrum of pristine copper exhibits a strong satellite structure, in contrast to the other spectra. This is due mostly to the superficial oxidised layer of the grains, composed of CuO and Cu–O–H groups. Milling with graphite for 14.4 ks almost completely removes these oxides, allowing niobium to interact with metallic copper and carbon (Fig. 4). Assignments of the multiplet structure are beyond the scope of this work and are not presented in Fig. 4. The subsequent addition of Nb powders to the Cu–C mixture leads to an increasing proportion of NbC as milling proceeds. X-ray diffractograms of mixtures with the two nominal compositions milled for 0.9 ks (Figs. 2 and 3) show a strong peak of Nb at about 38.5 (2θ °) that disappears when the milling time increases to 3.6 ks. The continuous increase in the proportion of NbC with milling time is demonstrated by the increase in the relative area of the NbC peak for both nanocomposites. Similar conclusions result from the XPS analysis. The relative intensity of the NbC component increases with milling time, reaching a plateau for $t > 28.8$ ks, while the intensity of NbO_2 decreases (Fig. 9).

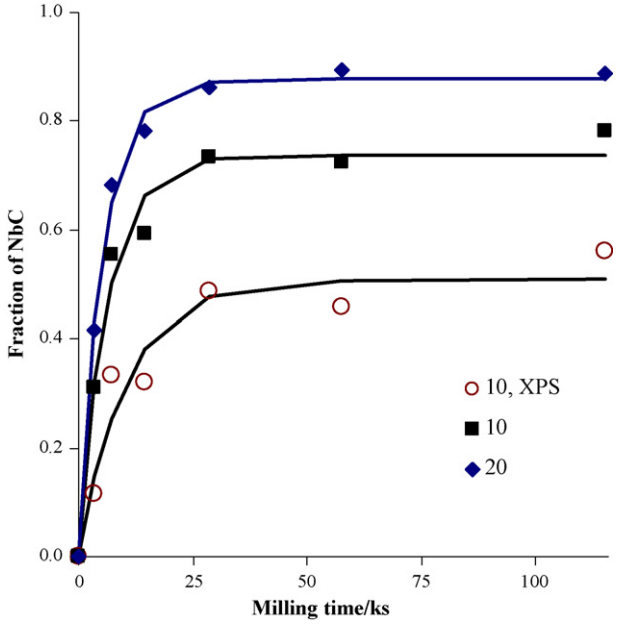

Fig. 8. Normalised fraction of NbC as a function of milling time for Cu 10 and 20 vol.% NbC obtained from XRD and XPS data. Symbols are experimental data and solid lines are the fitted exponential equation for each series of points. XPS experimental error ≤2%.

The relative atomic concentrations of Nb species correspond to the components fitted in the Nb 3d regions presented in Fig. 7. The quantitative analysis shows that the proportion of NbO_2 at 3.6 ks is nearly 90%, but this decreases by ~2/3 for longer milling times. Concomitantly, the proportion of NbC increases, while the proportion of Nb_2O_5 remains almost constant. Even after 115.2 ks of milling, only about 60% of the niobium reacted with carbon. Regarding copper, calculation of the Auger Parameter for milled samples indicates that the main line in the Cu $2p_{3/2}$ region, around 932 eV, can be assigned to Cu_2O (Cu^+). CuO, Cu–O–H and Cu^{2+} shake-up satellite are also present in milled powders but in smaller amounts than in the starting powder or in the 3.6 ks sample. The source of this oxygen is the surface oxide of the starting powders.

The kinetics of the evolution of mechanically alloyed Cu–NbC nanocomposites was studied by XPS and XRD. It is well known that MA induces solid-state chemical reactions.

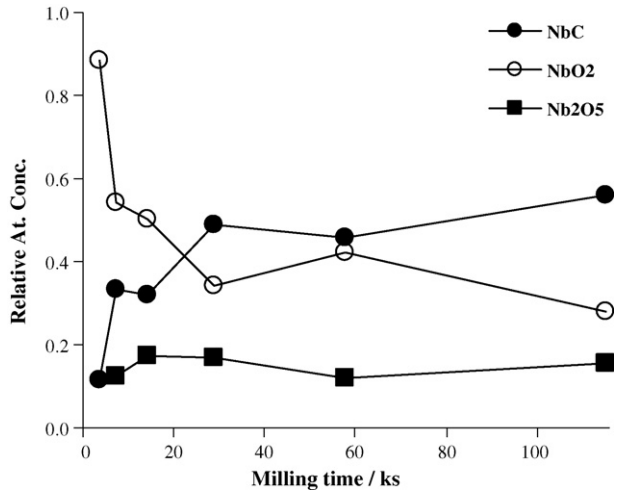

Fig. 9. Relative atomic concentrations of NbC, NbO_2 and Nb_2O_5 *vs.* milling time. The atomic concentrations correspond to the peaks fitted in the Nb 3d region obtained with the Al Kα source.

In fact, the results presented in this work show that MA with the experimental conditions used are a very effective method for synthesising Cu–NbC nanocomposites in a short time without additional heat treatment. The authors have not yet found kinetics studies in the literature describing the direct *in situ* formation of dispersion-strengthened copper alloys produced by MA without further treatments. A reasonable good fit of XPS and XRD experimental data to Eq. (3) was obtained (Fig. 8). The value of the rate constant, k, is similar for both XRD data sets ($\sim 1.8^{-1}\,ks^{-1}$), see Table 1; however, the authors have not found similar data in the literature to compare and discuss this value. The parameter a, the maximum proportion of NbC taking into consideration the concentration of reactants in the control powder mixture and the total reaction time, differs by about 16% for the present experiments. The values of the parameters estimated from XPS data are lower than those obtained from XRD. This difference is a consequence of the different sensitivities of these techniques. XPS probes the outermost layer of the powder particles (<10 nm) whereas XRD analyses a large volume of material. The presence of oxides at the surface attenuates the XPS signal.

The second purpose of pre-alloying Cu and graphite powder is directly related to NbC formation. Prior dispersion of carbon in the copper matrix can promote and enhance the reaction between Nb and C to form NbC. Such dispersion is possible because the solid solubility of carbon in copper is very low, about 7.4 ± 0.5 at. ppm at 1293 K [27]. This type of structure was previously observed for Cu–C powders [28,29] and TiC-dispersion-strengthened Cu alloys [8] prepared by MA. In fact, TEM analysis of Cu–C powders produced by MA [28] revealed the presence of low mass particles corresponding to carbon agglomerates in an amorphous state. The size of these agglomerates is less than 10 nm. They are uniformly distributed within the Cu grains, showing no preference for occupying positions near grain boundaries. A similar feature was observed by Dehm et al. [8] in TiC-dispersion-strengthened Cu alloys prepared by MA. Using HRTEM, the authors demonstrated that milling of pre-alloyed CuTi with graphite powders leads to the formation of carbon inclusions with diameters in the range 5–20 nm dispersed in the Cu-rich matrix. A detailed analysis proved that the carbon in these inclusions is amorphous or at least does not possess a well-defined crystalline structure. Taking these results into consideration, it seems reasonable to assume that the milled Cu–graphite powder prepared in the present work has a microstructure consisting of carbon nanoparticles dispersed in the copper matrix.

The addition of Nb to pre-alloyed powders can induce two solid state reactions leading to the formation of a CuNb solid solution and NbC, respectively. According to the Cu–Nb phase diagram the maximum solubility of Nb in solid Cu is about 0.2 at.% at 1353 K and no intermediate phases occur [30]. Nevertheless, previously published results [31,32] indicate that Cu–Nb solubility can be extended up to 10 at.% by milling Cu and Nb at liquid nitrogen temperature for 61.2 ks. This extension of solid solubility leads to an abnormal increase in the Cu lattice parameter. However, in the present research the lattice parameter of the Cu solid solution does not increase for milling times up to 28.8 ks [13]. Furthermore, a substantial amount of NbC is detected after 3.6 ks of milling and its proportion increases further up to at least 28.8 ks (Fig. 3). These findings indicate that the formation of a Cu(Nb) solid solution is not a realistic possibility. On the other hand, the equilibrium thermodynamic data of Gibbs free energy for NbC formation, $\Delta G_f = -137\,kJ\,mol^{-1}$ at 300 K [26], indicate that the reaction between C and Nb to form NbC is thermodynamically possible even at room temperature. The energy required to trigger this reaction is supplied to the system by the high-energy collisions due to the milling process, which causes intense plastic deformation of the particles, and seems to be sufficient to activate the reaction between C and Nb.

A possible mechanism to describe the formation of NbC is the following. According to several models proposed in the literature to explain the kinetics of mechanical alloying [33,34], lamellar structures are essential for the diffusive intermixing of solute atoms in the course of MA. In the present work a lamellar structure consisting of Nb/Cu–C or Nb/Cu–NbC–C is observed after 0.9 ks of milling, Fig. 1(a). These layers, of variable thickness, are fragmented into small particles and disappear with further milling. During the fragmentation process the Nb layers enter in contact with the carbon nanoparticles that are dispersed in the Cu matrix and a reaction between Nb and C occurs to form NbC. This reaction, thermodynamically favourable, probably occurs at the interfaces between Nb layers and C nanoparticles being activated by high-energy ball collisions. If this model is valid the NbC formation kinetics should depend strongly on the volume fraction of C and Nb particles in the matrix. This hypothesis is supported by the difference between the NbC volume fraction maxima observed for powders with 10 and 20 vol.% of NbC, see Fig. 8.

5. Conclusion

Cu-based nanocomposites with nominal compositions of 10 and 20 vol.% of NbC were produced *in situ* by mechanical alloying at room temperature. The kinetics of NbC *in situ* synthesis

in a copper matrix was studied with XRD and XPS. Results obtained with both techniques showed similar kinetics regarding the evolution of the NbC volume fraction for different milling times. Both XRD and XPS results show that the reaction is largely complete after 115.2 ks. A mechanism for the *in situ* formation of NbC nanoparticles in the copper matrix was proposed.

Acknowledgements

This work was supported by the program POCI 2010 – Medida IV.3 and the "Financiamento Plurianual of FCT-Fundação para a Ciência e a Tecnologia, Portugal.

References

[1] T. Takahashi, Y. Hashimoto, Mater. Trans. JIM 32 (1991) 389.
[2] J. Groza, J. Mater. Eng. Perform. 1 (1992) 113.
[3] J. Benjamin, Metall. Trans. A 1 (1970) 2943.
[4] C. Biseli, D.G. Morris, N. Randall, Scripta Metall. Mater. 30 (1994) 1327.
[5] K.R. Anderson, J.R. Groza, Metall. Mater. Trans. A 32 (2001) 1211.
[6] S.J. Dong, Y. Zhou, Y.W. Shi, B.H. Chang, Metall. Mater. Trans. A 33 (2002) 1275.
[7] B.R. Murphy, T.H. Courtney, Nanostruct. Mater. 4 (1994) 365.
[8] G. Dehm, J. Thomas, J. Mayer, T. Weissgarber, W. Pusche, C. Sauer, Philos. Mag. A 77 (1998) 1531.
[9] L. Weijie, D. Zhang, Z. Xiaonong, W. Renjie, T. Sakata, H. Mori, Scripta Mater. 44 (2001) 1069.
[10] R.H. Palma, A.O. Sepulveda, R.G. Espinoza, A.P. Zuniga, M.J. Dianez, J.M. Criado, M.J. Sayagues, Mater. Sci. Eng. A 384 (2004) 262.
[11] J.B. Correia, M.T. Marques, Adv. Mater. Forum II 455/456 (2004) 501.
[12] M.T. Marques, V. Livramento, J.B. Correia, A. Almeida, R. Vilar, Mater. Sci. Eng. A 399 (2005) 382.
[13] M.T. Marques, V. Livramento, J.B. Correia, A. Almeida, R. Vilar, J. Alloys Compd. 434/435 (2007) 481.
[14] Y. Taki, O. Takai, Thin Solid Films 316 (1998) 45.
[15] C.D. Wagner, A.V. Naumkin, A. Kraut-Vass, J.W. Allison, C.J. Powell, J.R. Rumble, NIST X-ray Photoelectron Spectroscopy Database, NIST Standard Reference Database 20, version 3.3, 2003. Web version: http://www.srdata.nist.gov/xps/.
[16] A. Darlinski, J. Halbritter, Surf. Interface Anal. 10 (1987) 223.
[17] A.N. MacInnes, A.R. Barron, J.J. Li, T.R. Gilbert, Polyhedron 13 (1994) 1315.
[18] J. Ghijsen, L.H. Tjeng, J. Vanelp, H. Eskes, J. Westerink, G.A. Sawatzky, M.T. Czyzyk, Phys. Rev. B 38 (1988) 11322.
[19] C.F. Miller, G.W. Simmons, R.P. Wei, Scripta Mater. 42 (2000) 227.
[20] G. van der Laan, C. Westra, C. Haas, G.A. Sawatzky, Phys. Rev. B 23 (1981) 4369.
[21] B.D. Cullity, Elements of X-Ray Diffraction, Addison-Wesley Publishing Company, Inc., Massachusetts, 1978, p. 133.
[22] M.W. Barsoum, T. El-Raghy, W.D. Porter, H. Wang, J.C. Ho, S. Chakraborty, J. Appl. Phys. 88 (2000) 6313.
[23] L.E. Toth, M. Ishikawa, Y.A. Chang, Acta Metall. 16 (1968) 1183.
[24] C.J. Smithells (Ed.), Metals Reference Book, Butterworths, London & Boston, 1976, p. 874.
[25] C. Suryanarayana, Prog. Mater. Sci. 46 (2001) 1.
[26] I. Barin, Thermochemical Data of Pure Substances, VCH Publishers, New York, NY, (USA), 1995, p. 1163.
[27] G.A. Lopez, E.J. Mittemeijer, Scripta Mater. 51 (2004) 1.
[28] P.A. Carvalho, I. Fonseca, M.T. Marques, J.B. Correia, R. Vilar, Mater. Sci. Technol. 22 (2006) 673.
[29] M.T. Marques, J.B. Correia, O. Conde, Scripta Mater. 50 (2004) 963.
[30] T.B. Massalski (Ed.), Binary Alloy Phase Diagrams, William W. Scott, Jr., Ohio, 1986, p. 559.
[31] E. Botcharova, M. Heilmaier, J. Freudenberger, G. Drew, D. Kudashow, U. Martin, L. Schultz, J. Alloys Compd. 351 (2003) 119.
[32] E. Botcharova, J. Freudenberger, L. Schultz, J. Alloys Compd. 365 (2004) 157.
[33] D. Das, P.P. Chatterjee, I. Manna, S.K. Pabi, Scripta Mater. 41 (1999) 861.
[34] F. Delogu, G. Cocco, J. Mater. Synth. Proc. 8 (2000) 271.